

The Structure and Energetics of ^3He and ^4He Nanodroplets Doped with Alkaline Earth Atoms[†]

Alberto Hernando,[§] Ricardo Mayol,[§] Martí Pi,[§] Manuel Barranco,^{*,§} Francesco Ancilotto,[#] Oliver Bünermann,[‡] and Frank Stienkemeier[‡]

Departament ECM, Facultat de Física, and IN²UB, Universitat de Barcelona, Diagonal 647, 08028 Barcelona, Spain, INFN-DEMOCRITOS and Dipartimento di Fisica “G. Galilei”, Università di Padova, via Marzolo 8, I-35131 Padova, Italy, and Physikalisches Institut, Universität Freiburg, Hermann-Herder Str. 3, D-76104 Freiburg, Germany

Received: January 8, 2007; In Final Form: March 5, 2007

We present systematic results, based on density functional calculations, for the structure and energetics of ^3He and ^4He nanodroplets doped with alkaline earth atoms. We predict that alkaline earth atoms from Mg to Ba go to the center of ^3He drops, whereas Ca, Sr, and Ba reside in a deep dimple at the surface of ^4He drops, and Mg is at their center. For Ca and Sr, the structure of the dimples is shown to be very sensitive to the He–alkaline earth pair potentials used in the calculations. The $5s5p \leftarrow 5s^2$ transition of strontium atoms attached to helium nanodroplets of either isotope has been probed in absorption experiments. The spectra show that strontium is solvated inside ^3He nanodroplets, supporting the calculations. In the light of our findings, we emphasize the relevance of the heavier alkaline earth atoms for analyzing mixed ^3He – ^4He nanodroplets, and in particular, we suggest their use to experimentally probe the ^3He – ^4He interface.

1. Introduction

Optical investigations of impurities in liquid helium have drawn considerable attention in the past.¹ In recent years, experiments involving helium nanodroplets have added new input into the interaction of atomic impurities with a superfluid helium environment.^{2,3} In particular, the shifts of the electronic transition lines represent a very useful observable to determine the location of the foreign atom attached to a helium drop.

While most impurities are found to reside in the interior of helium droplets,^{4–7} it is well-established that alkali atoms, due to their weak interaction with helium, reside in a “dimple” at the surface of the drop for both helium isotopes.^{8–10} The question of solvation versus surface location for an impurity atom in liquid He can be addressed within the model of ref 11, where a simple criterion has been proposed to decide whether surface or solvated states are energetically favored. An adimensional parameter λ can be defined in terms of the impurity–He potential well depth ϵ and the minimum position r_{min} , namely, $\lambda \equiv \rho \epsilon r_{\text{min}} / (2^{1/6} \sigma)$, where ρ and σ are the density and surface tension of bulk liquid He, respectively. The threshold for solvation in ^4He is¹¹ $\lambda \sim \lambda_0$, with $\lambda_0 = 1.9$. When $\lambda < \lambda_0$, a stable state of the impurity on the droplet surface is expected, whereas when $\lambda > \lambda_0$, the impurity is likely to be solvated in the interior of the droplet. Impurities such as neutral alkali atoms, that weakly interact with helium, are characterized by values of λ much smaller than the above threshold; their stable state is thus expected to be on the surface of the droplet, as experimentally found.

The shape of the impurity–He interaction potential, however, is not given consideration by this model. For cases in which the value of λ does not lie near (say, within 0.5) the solvation threshold λ_0 , the shape of the potential surface does not need to be taken into account, as the model is predictive outside of this threshold window. However, for values which lie close to λ_0 , consideration of the shape of the potential energy surface, as well as the well depth and equilibrium internuclear distance, is mandatory, and more detailed calculations are needed to ascertain whether the impurity is solvated or not. It is worth noticing that the above criterion works for either helium isotope, although so far, it has been applied to ^4He because experimental data for ^3He only appeared recently.^{9,12–14}

Among simple atomic impurities, alkaline earth (Ake) atoms play a unique role. While, for example, all alkali atoms reside on the surface and all noble gas atoms reside in the interior of drops made of either isotope,¹⁵ the absorption spectra of heavy alkaline earth atoms Ca, Sr, and Ba attached to a ^4He cluster clearly support an outside location of Ca and Sr¹⁶ and likely also of Ba,¹⁷ whereas for the lighter Mg atom, the experimental evidence shows that it resides in the interior of the ^4He droplets.^{18,19}

According to the magnitude of the observed shifts, the dimple in the case of alkaline earth atoms is thought to be more pronounced than in the case of alkalis, indicating that alkaline earth atoms reside deeper inside the drop than alkali atoms. This will be corroborated by density functional calculations presented in the Theoretical Results. Laser-induced fluorescence results for Ca atoms in liquid ^3He and ^4He have been recently reported²⁰ and have been analyzed using a vibrating “bubble model” and fairly old Ca–He pair potentials based on pseudopotential SCF/CI calculations.²¹

Applying the simple criterion described above, Ca and Sr appear to be barely stable in their surface location with respect

[†] Part of the “Roger E. Miller Memorial Issue”.

* To whom correspondence should be addressed. E-mail: manuel@ecm.ub.es. Phone: +34 93 402 1184. Fax: +34 93 402 1198.

[§] Universitat de Barcelona.

[#] Università di Padova.

[‡] Universität Freiburg.

TABLE 1: The λ Parameter for the Alkaline Earth Atoms and Pair Potentials Used in This Work

	λ	
	^3He	^4He
Mg ^a	4.73	2.60
Ca ^a	3.78	2.08
Ca ^b	3.71	2.04
Ca ^c	4.02	2.21
Ca ^d	4.52	2.49
Sr ^b	3.48	1.92
Ba ^b	3.15	1.73

^a Ref (30). ^b Ref (29). ^c Ref (32). ^d Ref (31).

to the bulk one,²² as reflected in the λ values collected in Table 1, which are close to λ_0 for these doped ^4He systems. This borderline character for the solvation properties of these impurities implies that detailed calculations are required to understand the results of spectroscopic studies on alkaline-earth-doped He droplets. In particular, high-quality impurity–He pair interaction potentials are required since even relatively small inaccuracies in these potentials, which are often not known with a sufficient precision, may yield wrong results.

We present here a systematic study for helium drops made of each isotope, having a number of atoms large enough to make them useful for the discussion of experiments on laser-induced fluorescence (LIF) or beam depletion (BD) spectroscopy or for the discussion of other physical phenomena involving these systems, such as interatomic Coulombic decay.^{23,24} We also discuss the dependence of the structural properties on the cluster size. Some of this information is also experimentally available.¹⁷ After a brief explanation of the experiment, results are presented for strontium on helium nanodroplets that further support the calculations.

This work is organized as follows. In Section 2, we briefly describe the density functional plus alkaline earth–He potential approach employed here, as well as some technical details. Doped drops calculations are presented and discussed in Section 3, while the experimental results are discussed in Section 4, and an outlook is presented in Section 5.

2. Density Functional Description of Helium Nanodroplets

Since the pioneering work of Stringari and co-workers,²⁵ density functional (DF) theory has been used in many studies on liquid helium in confined geometries and found to provide a quite accurate description of the properties of inhomogeneous liquid He (see, e.g., ref 15 and references therein).

The starting point is to write the energy of the system as a functional of the He particle density ρ

$$E[\rho] = \int d\mathbf{r} \epsilon(\rho) + \int d\mathbf{r}' \rho(\mathbf{r}') V_{\text{Ake-He}}(|\mathbf{r} - \mathbf{r}'|) \quad (1)$$

where $\epsilon(\rho)$ is the He energy density per unit volume, and $V_{\text{Ake-He}}$ is the alkaline earth–helium pair potential. The impurity is thus treated as a fixed external potential. Addressing the lightest alkaline earth, Be, for which a fairly recent Be–He is available,²⁶ would likely require treatment of this atom as a quantum particle instead of as an external potential.¹⁵

For ^4He , we have used the Orsay–Trento functional²⁷ and, for ^3He , the one described in ref 28 and references therein. These functionals have been used in our previous work on helium drops doped with alkali atoms^{9,10} as well as in many other theoretical works. The results discussed in the following have been mostly obtained using the potentials of ref 29 (Ca, Sr,

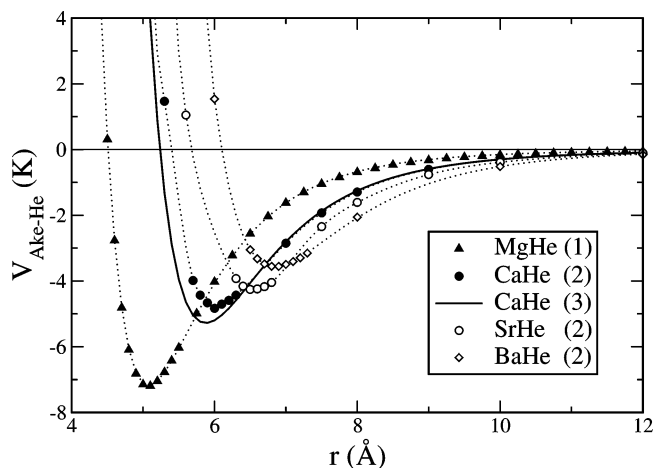


Figure 1. Alkaline earth–He pair potentials used in this work to obtain the ground-state structure of doped helium drops: (1) ref 30; (2) ref 29; (3) ref 32.

and Ba) and of ref 30 (Mg, for which the pair potentials of refs 26 and 30 are similar). For Ca, we have also tested other potentials available in the literature^{26,30,31} as well as the unpublished potential of Meyer³² we had employed in our previous work.²²

Figure 1 shows the pair potentials used in this work. From this figure, one may anticipate that $\text{Ca}@^4\text{He}_N$ drops described using the potential of ref 32 display deeper dimples than the same drops described with the potential of ref 29. We want to point out that the Ca–He potentials of refs 26 and 30 are very similar to that of ref 29 and should yield equivalent results. Contrarily, we have found that the potential of ref 31 is more attractive, causing the Ca atom to be drawn to the center of the $^4\text{He}_N$ drop, in contrast with the experimental findings.¹⁷

For a number N of helium atoms in the drop, we have solved the Euler–Lagrange equation, which results from the variation of $E[\rho]$ at constant N

$$\frac{\delta \epsilon}{\delta \rho} + V_{\text{Ake-He}} = \mu \quad (2)$$

where μ is the helium chemical potential, whose value is determined self-consistently by imposing the auxiliary condition $\int d\mathbf{r} \rho(\mathbf{r}) = N$ during the iterative minimization.

When the impurity resides off center (as in the case of a dimple structure), the system is axially symmetric. Despite this symmetry, we have solved eq 2 in Cartesian coordinates because this allows us to use fast Fourier transform techniques³³ to efficiently compute the convolution integrals entering the definition of $\epsilon(\rho)$, that is, the mean field helium potential and the coarse-grained density needed to evaluate the correlation term in the density functional.²⁷ We have found this procedure to be faster and more accurate than convoluting by direct integration using cylindrical coordinates.

We have used an imaginary time method^{34,35} to solve eq 2, after having discretized it using 13-point formulas for the spatial derivatives. The mesh used to discretize ρ in space is chosen so that the results are stable against small changes of the mesh step.

3. Theoretical Results

We start a typical calculation by placing the impurity close to the surface of the He droplet. Depending on the studied impurity and/or the He isotope, during the functional minimization, the alkaline earth atom is either driven to the interior of

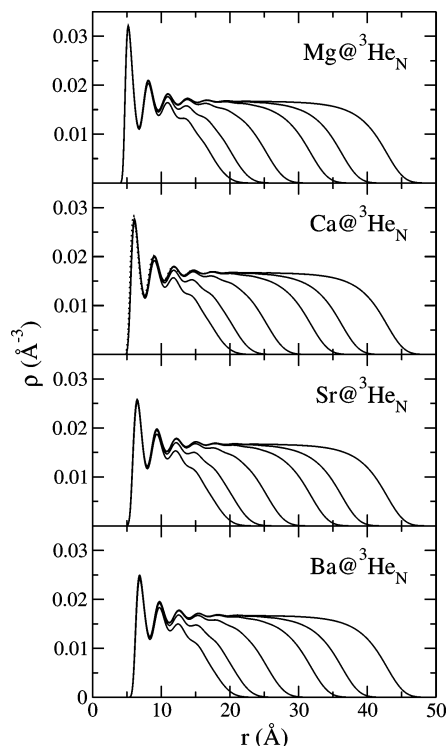


Figure 2. Density profiles for $^3\text{He}_N$ drops doped with Mg, Ca, Sr, and Ba, for $N = 300, 500, 1000, 2000, 3000,$ and 5000 . The dotted line in the Ca panel corresponds to $\text{Ca}@^3\text{He}_{5000}$ calculated with the pair potential of ref 32. Drops doped with Ca, Sr, and Ba have been calculated using the pair potentials of ref 29, and drops doped with Mg were calculated using the pair potential of ref 30.

the droplet,³⁶ or it remains trapped in a more or less pronounced dimple on its surface.

In the case of ^3He , we find that for all of the alkaline earth atoms investigated, the stable state is always the one where the impurity is in the center of the cluster. This is consistent with the associated large λ values; see Table 1. Figure 2 shows the density profiles for $\text{Mg}@^3\text{He}_N$, $\text{Ca}@^3\text{He}_N$, $\text{Sr}@^3\text{He}_N$, and $\text{Ba}@^3\text{He}_N$ for $N = 300, 500, 1000, 2000, 3000,$ and 5000 . For $\text{Ca}@^3\text{He}_{5000}$, we also show the profile obtained with the pair potential of ref 32 (dotted line). Several solvation shells are clearly visible. The number of ^3He atoms below the first solvation peak for the $N = 5000$ drop is about 19 for Mg, 22 for Ca, 26 for Sr, and 27 for Ba. The differences in the location and height of the first solvation peak are a simple consequence of the different depth and equilibrium distance of the corresponding pair potentials. It is interesting to see the building up of the drop structure around the impurity that, as it is well-known,⁵ only causes a large but localized effect on the drop structure.

The bottom panel of Figure 3 shows the corresponding solvation energies, defined as the energy differences

$$S_N(\text{Ake}) = E(\text{Ake}@^3\text{He}_N) - E(^3\text{He}_N) \quad (3)$$

with an equivalent definition for ^4He drops. The more attractive Ca–He pair potential of ref 32 yields, on average, a solvation energy about 13 K larger as compared with that obtained with the pair potential of ref 29, despite the fact that the density profiles look fairly similar; see Figure 2.

In the case of Ca and Sr atoms in ^4He drops, whose λ values are close to the threshold for solvation λ_0 (see Table 1), we have found that, for both dopants, the minimum energy configuration is a dimple state at the surface, although the energy

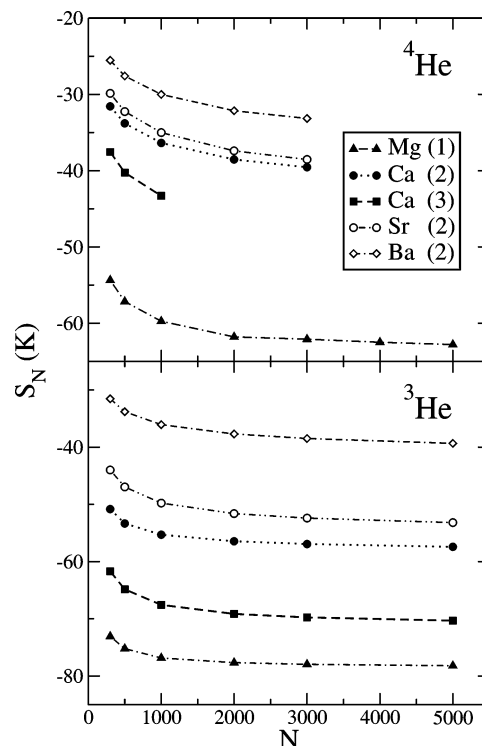


Figure 3. Top panel: solvation energies (K) for doped $^4\text{He}_N$ drops. Results were obtained using the following pair potentials: (1) from ref 30; (2) from ref 29; (3) from ref 32. Bottom panel: same as the top panel for doped $^3\text{He}_N$ drops. The lines are drawn to guide the eye.

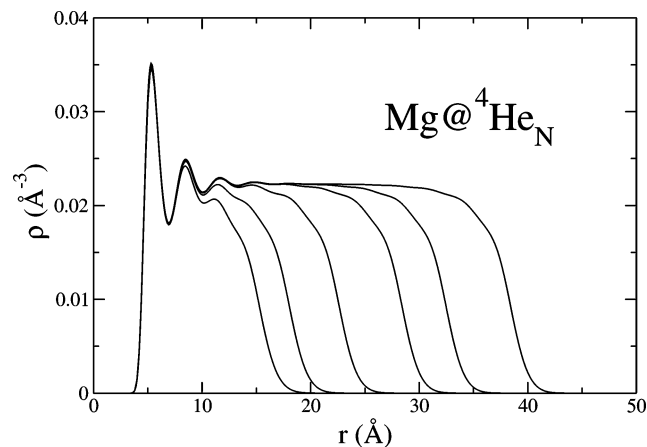


Figure 4. Density profiles for $\text{Mg}@^4\text{He}_N$ drops for $N = 300, 500, 1000, 2000, 3000,$ and 5000 . Results were obtained using the pair potential of ref 30.

difference between the surface and the solvated states is fairly small for both dopants. For $\text{Ca}@^4\text{He}_{300}$, this difference is 3.4 K using Meyer’s potential²² and 12.0 K using that of ref 29. The homologous result for $\text{Sr}@^4\text{He}_{300}$ is 22.7 K. These energy differences have to be compared with the total energy of the $^4\text{He}_{300}$ drop, which is about -1384 K.

We have also confirmed by DF calculations the surface state of $\text{Ba}@^4\text{He}_N$ and the solvated state of $\text{Mg}@^4\text{He}_N$, both suggested by the corresponding λ values in Table 1. This is illustrated in Figure 4 for Mg and in Figure 5 for Ca, Sr, and Ba. The dimple depth ξ , defined as the difference between the position of the dividing surface at $\rho = \rho_b/2$, where ρ_b is the bulk liquid density, with and without impurity, respectively, is shown in Figure 6 as a function of N . The structure of the dimple is different for different alkaline earth atoms, being shallower for Ba and more pronounced for Ca. We recall that the ξ values for $\text{Na}@^3\text{He}_{2000}$

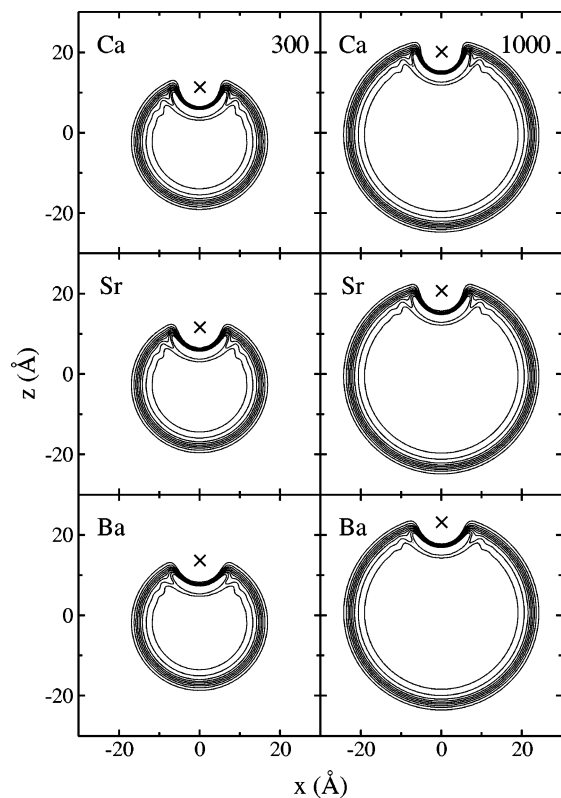


Figure 5. Equidensity lines on a symmetry plane for ${}^4\text{He}_N$ drops with $N = 300$ (left panels) and 1000 (right panels) doped with Ca, Sr, and Ba. The lines span the surface region between 0.9 and $0.1 \rho_b$ in $0.1 \rho_b$ steps, where ρ_b is the bulk liquid density 0.0218 \AA^{-3} . The cross indicates the location of the alkaline earth atom in the dimple. Results were obtained using the pair potentials of ref 29.

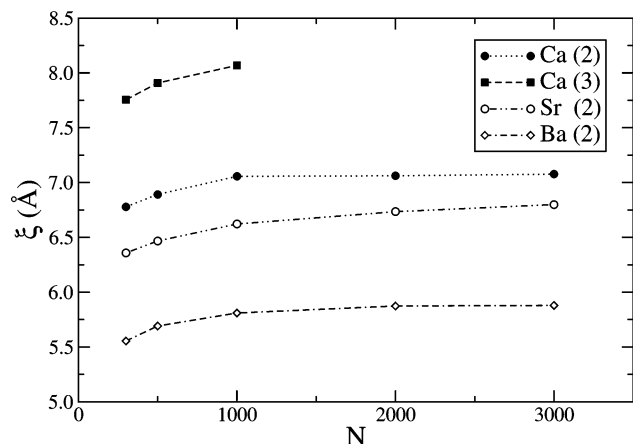


Figure 6. Depth of the dimples (ξ) created in ${}^4\text{He}_N$ drops obtained using the following pair potentials: (2) from ref 29 for Ba (diamonds), Sr (circles), and Ca (solid dots) atoms; (3) from ref 32 for Ca (squares). The lines are drawn to guide the eye.

and $\text{Na}@{}^4\text{He}_{2000}$ are 4.5 and 2.1 \AA , respectively.⁹ The dimple depths for alkaline atoms are thus much smaller than those for alkaline earth atoms, as also indicated by LIF experiments.^{2,9,16,17} The dependence of the dimple depth with the alkaline earth atom size, characterized by the radial expectation value R_{Ake} of the valence electrons,³⁷ is shown in Figure 7. This figure is consistent with the increasing bulk-to-surface ratio of the line shifts as the size of the dopant atom increases.¹⁷

The “solvation” energies for these alkaline earth atoms in ${}^4\text{He}$ drops are displayed in the top panel of Figure 3. As in the case of ${}^3\text{He}$ drops discussed before, the stronger the Ake–He pair potential (see Figure 1), the more negative $S_N(\text{Ake})$. In the

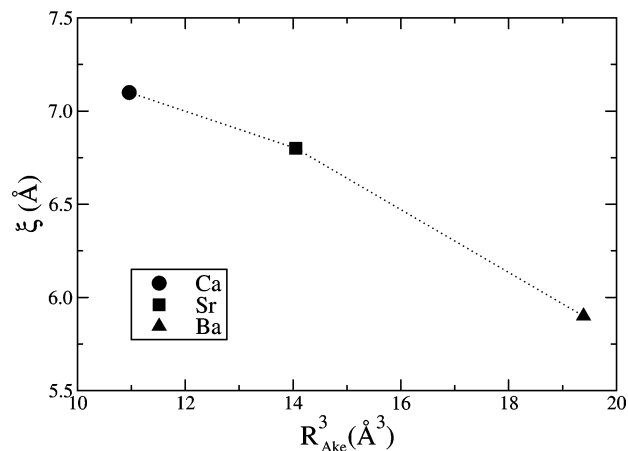


Figure 7. Depth of the dimples (ξ) created in ${}^4\text{He}_{3000}$ drops by Ba, Sr, and Ca atoms as a function of the atomic size R_{Ake}^3 , using the pair potentials of ref 29. The line is drawn to guide the eye.

case of $\text{Ca}@{}^4\text{He}_N$ and $\text{Sr}@{}^4\text{He}_N$, the energies are very similar, and so are the dimple depths shown in Figure 6. It is worth seeing the different behavior of S_N as a function of N for each helium isotope. In the case of ${}^3\text{He}$, once the first two to three solvation shells are fully developed, S_N quickly saturates, and for this reason, it changes only by 12% (Ca) and 17% (Sr) from $N = 300$ to 5000. For the same reason, spectroscopic shifts are expected to be N independent for drops made of more than a few hundred ${}^3\text{He}$ atoms. When the impurity is at the surface, sizable curvature effects appear even for a few thousand atoms drops. This shows up not only in the change of S_N , which is about 22% for Ca and 24% for Sr in the same N range as before, but also in the spectroscopic shifts, which still depend on N below $N \sim 3000$ (see, e.g., ref 17). This illustrates the need of large drops for carrying out spectroscopic shift calculations to attempt a detailed comparison with experiments.

4. Experimental Results

To support the DF calculations, the $5s5p \text{ } {}^1\text{P}_1^0 \leftarrow 5s^2 \text{ } {}^1\text{S}_0$ transition of strontium on nanodroplets made of either helium isotope has been experimentally investigated. Although calcium appears to be most favorable, we are, so far, restricted to excitation spectra of strontium attached to helium droplets because of the limited tuning range of our lasers. Calcium will be addressed in a future experiment. The experiments were performed in a helium droplet machine applying laser-induced fluorescence, as well as beam depletion and photoionization (PI) spectroscopy. A detailed description of the experimental setup is presented elsewhere.¹⁷ Modifications include a new droplet source to reach the lower temperatures needed for generating ${}^3\text{He}$ droplets.⁹ In short, gas of either helium isotope is expanded under supersonic conditions from a nozzle, forming a beam of droplets traveling freely in high vacuum. The helium stagnation pressure in the droplet source is 20 bar, and a nozzle of $5 \mu\text{m}$ diameter has been used. The nozzle temperature has been stabilized to 12 and 15 K to form ${}^3\text{He}$ and ${}^4\text{He}$ droplets, respectively. These conditions result in an average droplet size of ~ 5000 helium atoms.⁷

The droplets are doped downstream using the pick-up technique; in a heated scattering cell, an appropriate vapor pressure of strontium is established so that droplets pick up one single atom on average when passing the cell. LIF as well as PI and BD absorption spectra of the doped droplet beam can be recorded upon electronic excitation using a pulsed nanosec-

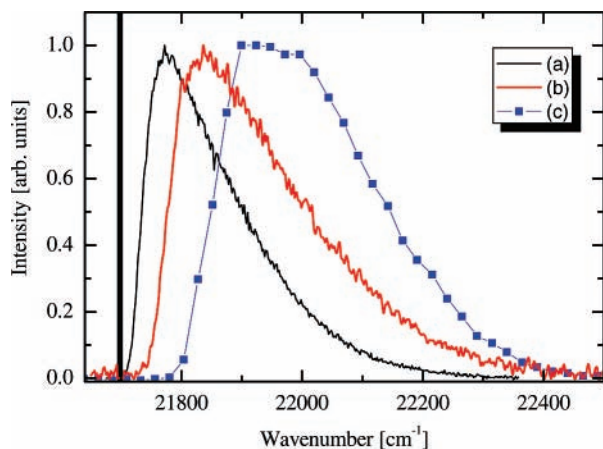


Figure 8. Spectra of the Sr $5s5p\ ^1P_1^0 \leftarrow 5s^2\ ^1S_0$ transition: (a) ^4He drops, (b) ^3He drops, and (c) bulk ^4He .³⁹ The vertical bar corresponds to the atomic line.

ond dye laser. LIF is recorded with a photomultiplier tube. In the case of PI, the photons of an excimer laser ionize the excited atoms in a one-photon step. The ions are, afterward, detected by a channeltron. For the beam depletion measurement, a Langmuir–Taylor surface ionization detector has been used.³⁸

We show here only the results obtained using LIF because a much better signal-to-noise ratio was achieved when compared to the PI and BD spectra for strontium-doped clusters. In the case of PI, the reason probably is the tendency of the just-formed strontium ions not to desorb from the droplet like, for example, alkali atoms do. Since the detection efficiency of our PI detector is considerably decreased for high masses, the detection of the ion + droplet complex is small. A decreased desorption mechanism also diminishes the sensitivity of BD techniques. However, the PI/BD measurements give identical results when compared to the LIF spectra.

Figure 8 shows the measured spectra of the $5s5p\ ^1P_1^0 \leftarrow 5s^2\ ^1S_0$ transition of strontium atoms on droplets of $^3\text{He}/^4\text{He}$ compared to that in bulk ^4He .³⁹ All three spectra show a broad asymmetric line, blue shifted from the atomic gas-phase absorption. The differences of the shifts for ^4He drops and bulk ^4He immediately confirm the surface location of the strontium atoms.¹⁶ In the case of bulk ^4He , the absorption is far more blue shifted, and the width is considerably wider. The shift can be explained within the bubble model, see, for example, refs 1 and 20 and references therein, and results from repulsion of the helium environment against spatial enlargement of the electronic distribution of the excited state. The shift in bulk helium is larger than that in droplets because the dopant is completely surrounded by helium, whereas it is not when it is located at the surface of drops.

Table 2 summarizes the experimentally determined shifts of the first electronic transition of strontium and calcium in helium droplets, as well as the measurements in bulk helium for both isotopes. As compared to ^4He drops, the absorption maximum in the case of ^3He drops is shifted 60 cm^{-1} further to the blue, and the width increases from 180 to 220 cm^{-1} .

At first glance, it is not obvious from the recorded spectra in ^3He drops whether the strontium atom is in a surface state or if it is solvated inside the droplets. It is worth mentioning that Moriwaki et al. performed similar measurements in bulk helium.²⁰ They have compared the absorption spectra of the $4s4p\ ^1P_1^0 \leftarrow 4s^2\ ^1S_0$ transition of calcium in bulk ^3He and ^4He and have found a much smaller blue shift in the case of ^3He (about 55%; see Table 2), which could again be explained within the

TABLE 2: Experimental Shifts of the First Electronic Transition of Ca and Sr Atoms in Bulk Helium as Well as in Drops^a

	bulk		drop	
	^4He	^3He	^4He	^3He
Ca				
shift (cm^{-1})	203 ^c	112 ^c	72 ^b	
fwhm (cm^{-1})	297 ^c	245 ^c	173 ^b	
Sr				
shift (cm^{-1})	240 ^d		80	140
fwhm (cm^{-1})	287 ^d		180	220

^a The values for $\text{Sr}@^3\text{He}_N$ are from this work. Previous experiments, carried out only for $\text{Sr}@^4\text{He}_N$, showed the same shifts.¹⁷ ^b Ref (17). ^c Ref (20). ^d Ref (39).

bubble model; the reduced shift just results from the lower density of liquid ^3He . A similar quantitative effect should be expected for strontium, especially in view of the reported DF calculations.

Consistent with this expectation is that, in our experiments, the measured shift of Sr in ^3He droplets, 140 cm^{-1} , is about 58% of the value corresponding to Sr in bulk ^4He , 240 cm^{-1} .³⁹ We can safely argue that the shift determined in ^3He droplets should sensibly coincide with the expected value for bulk ^3He , indicating complete solvation of strontium atoms in ^3He droplets, as predicted by DF calculations.

5. Summary and Outlook

In this work, we have presented detailed results for the structure and energetics of helium drops doped with Mg, Ca, Sr, and Ba alkaline earth atoms. We have found that these atoms are solvated in the case of ^3He drops and reside in surface dimples in the case of ^4He drops, with the sole exception of $\text{Mg}@^4\text{He}_N$, which is also solvated. This yields a fairly complete physical picture, from the theoretical viewpoint, of the structure and energetics of helium drops doped with alkaline earth atoms. The experimental spectrum of strontium atoms in ^4He and ^3He droplets confirms the DF calculations. Moreover, since the spectroscopic shift is sensitive to the shape/depth of the surface dimple, a comparison between experimental and calculated line shifts could provide a sensible test on the accuracy of available pair potentials. We want to stress again that accurate pair potentials are needed to quantitatively reproduce the experimental results, especially when the solvation properties of the impurity are such that they yield values of λ close to the threshold value λ_0 .

The different solvation behavior of the heavier alkaline earth atoms in ^3He and ^4He drops offers the unique possibility of using them to study mixed drops at very low temperatures, in particular the ^3He – ^4He interface. It is known that, below the tricritical point at $\sim 0.87\text{ K}$,⁴⁰ ^3He has a limited solubility in ^4He , segregating for concentrations larger than a critical value. This segregation also appears in mixed droplets,^{12,41,42} producing a shell structure in which a core, essentially made of ^4He atoms, is coated by ^3He that is hardly dissolved into the ^4He core, even when the number of ^3He atoms is very large.⁴¹ Due to this particular structure that pertains to medium to large size droplets, strongly attractive impurities reside in the ^4He core, being effected very little by the outer ^3He shell, whereas weakly attractive impurities, like alkali atoms, should still reside in the surface of the droplet, irrespective of the existence of the ^4He core. Contrarily, Ca, Sr, and Ba impurities will be sunk into the fermionic component up to reaching the ^3He – ^4He interface if the appropriate number of atoms of each isotope is chosen.

This will offer the possibility of studying the ^3He – ^4He interface and a richer alkaline earth atom environment. We are, at present, generalizing the DF approach that we have used in the past⁴¹ to address this more demanding and promising new aspect of the physics of doped helium droplets. On the experimental side, calcium spectra will be accessible in forthcoming experiments. We want to point out that mixed droplets doped with alkali atoms have been already detected in our previous experiments¹⁴ and that systematic experiments on alkaline-earth-doped mixed droplets will be performed in the future.

Acknowledgment. We would like to thank Josef Tiggesbäumker and Marek Krośnicki for useful correspondence. This work has been performed under Grant No. FIS2005-01414 from DGI, Spain (FEDER), Grant 2005SGR00343 from Generalitat de Catalunya, and under the HPC-EUROPA project (RII3-CT-2003-506079), with the support of the European Community-Research Infrastructure Action under the FP6 “Structuring the European Research Area” Programme.

References and Notes

- (1) Tabbert, B.; Günther, H.; zu Putlitz, G. *J. Low Temp. Phys.* **1997**, *109*, 653.
- (2) Stienkemeier, F.; Vilesov, A. F. *J. Chem. Phys.* **2001**, *115*, 10119.
- (3) Stienkemeier, F.; Lehmann, K. K. *J. Phys. B: At. Mol. Opt. Phys.* **2006**, *39*, R127.
- (4) Barnett, R. N.; Whaley, K. B. *Phys. Rev. A* **1993**, *47*, 4082.
- (5) Dalfovo, F. *Z. Phys. D: At., Mol. Clusters* **1994**, *29*, 61.
- (6) Callegari, C.; Lehmann, K. K.; Schmied, R.; Scoles, G. *J. Chem. Phys.* **2001**, *115*, 10090.
- (7) Toennies, J. P.; Vilesov, A. F. *Angew. Chem., Int. Ed.* **2004**, *43*, 2622.
- (8) Ancilotto, F.; Cheng, E.; Cole, M. W.; Toigo, F. *Z. Phys. B: Condens. Matter* **1995**, *98*, 323.
- (9) Stienkemeier, F.; Bünermann, O.; Mayol, R.; Ancilotto, F.; Barranco, M.; Pi, M. *Phys. Rev. B* **2004**, *70*, 214509.
- (10) Mayol, R.; Ancilotto, F.; Barranco, M.; Pi, M.; Bünermann, O.; Stienkemeier, F. *J. Low Temp. Phys.* **2005**, *138*, 229.
- (11) Ancilotto, F.; Lerner, P. B.; Cole, M. W. *J. Low Temp. Phys.* **1995**, *101*, 1123.
- (12) Grebenev, S.; Toennies, J. P.; Vilesov, A. F. *Science* **1998**, *279*, 2083.
- (13) Harms, J.; Toennies, J. P.; Barranco, M.; Pi, M. *Phys. Rev. B* **2001**, *63*, 184513.
- (14) Bünermann, O. Ph.D. Thesis, University of Bielefeld, Germany, 2006.
- (15) Barranco, M.; Guardiola, R.; Hernández, S.; Mayol, R.; Pi, M. *J. Low Temp. Phys.* **2006**, *142*, 1.
- (16) Stienkemeier, F.; Meier, F.; Lutz, H. O. *J. Chem. Phys.* **1997**, *107*, 10816.
- (17) Stienkemeier, F.; Meier, F.; Lutz, H. O. *Eur. Phys. J. D* **1999**, *9*, 313.
- (18) Reho, J.; Merker, U.; Radcliff, M. R.; Lehmann, K. K.; Scoles, G. *J. Chem. Phys.* **2000**, *112*, 8409.
- (19) Przystawik, A. Ph.D. Thesis, University of Rostock, Germany, 2007.
- (20) Moriwaki, Y.; Morita, N. *Eur. Phys. J. D* **2005**, *33*, 323.
- (21) Czuchaj, E.; Rebentrost, F.; Stoll, H.; Preuss, H. *Chem. Phys. Lett.* **1991**, *182*, 191.
- (22) Ancilotto, F.; Barranco, M.; Pi, M. *Phys. Rev. Lett.* **2003**, *91*, 105302.
- (23) Cederbaum, L. S.; Zobeley, J.; Tarantelli, F. *Phys. Rev. Lett.* **1997**, *79*, 4778.
- (24) Kryzhevoi, N. V.; Averbukh, V.; Cederbaum, L. S. *Phys. Rev. Lett.* **2006**, submitted for publication.
- (25) Stringari, S.; Treiner, J. *J. Chem. Phys.* **1987**, *87*, 5021.
- (26) Partridge, H.; Stallcop, J. R.; Levin, E. *J. Chem. Phys.* **2001**, *115*, 6471.
- (27) Dalfovo, F.; Lastri, A.; Pricapenko, L.; Stringari, S.; Treiner, J. *Phys. Rev. B* **1995**, *52*, 1193.
- (28) Mayol, R.; Pi, M.; Barranco, M.; Dalfovo, F. *Phys. Rev. Lett.* **2001**, *87*, 145301.
- (29) Lovallo, C. C.; Klobukowski, M. *J. Chem. Phys.* **2004**, *120*, 246.
- (30) Hinde, R. J. *J. Phys. B: At. Mol. Opt. Phys.* **2003**, *36*, 3119.
- (31) Czuchaj, E.; Krośnicki, M.; Stoll, H. *Chem. Phys.* **2003**, *292*, 101.
- (32) Meyer, W. Personal communication.
- (33) Frigo, M.; Johnson, S. G. The Design and Implementation of FFTW3. *Proc. IEEE* **2005**, *93*, 216.
- (34) Press, W. H.; Teulosky, S. A.; Vetterling, W. T.; Flannery, B. P. *Numerical Recipes in Fortran 77: The Art of Scientific Computing*; Cambridge University Press: Cambridge, U.K., 1999.
- (35) Ancilotto, F.; Austing, D. G.; Barranco, M.; Mayol, R.; Muraki, K.; Pi, M.; Sasaki, S.; Tarucha, S. *Phys. Rev. B* **2003**, *67*, 205311.
- (36) Since we treat the impurity as an infinitely heavy particle, what actually occurs is that, during the functional minimization, helium is drawn towards the impurity, embedding it until a final, lowest energy configuration is reached, where the impurity sits in the center of the droplet. Numerically, the process is optimized by computing the force acting on the impurity and moving it in the direction of that force; see, for example, ref 8.
- (37) Desclaux, J. P. *At. Data Nucl. Data Tables* **1973**, *12*, 311.
- (38) Stienkemeier, F.; Wewer, M.; Meier, F.; Lutz, H. O. *Rev. Sci. Instrum.* **2000**, *71*, 3480.
- (39) Bauer, H.; Beau, M.; Friedel, B.; Marchand, C.; Miltner, K. *Phys. Lett. A* **1990**, *146*, 134.
- (40) Edwards, D. O.; Pettersen, M. S. *J. Low Temp. Phys.* **1992**, *87*, 473.
- (41) Pi, M.; Mayol, R.; Barranco, M. *Phys. Rev. Lett.* **1999**, *82*, 3093.
- (42) Fantoni, S.; Guardiola, R.; Navarro, J.; Zucker, A. *J. Chem. Phys.* **2005**, *123*, 054503.